Smart Structures and Systems, Vol. 6, No. 7 (2010) 793-810
DOI: http://dx.doi.org/10.12989/sss.2010.6.7.793

On the control of vibratory MEMS gyroscopes

S. Choura[1], N. Aouni[2] and S. El-Borgi*[3]

[1]*Micro-Electro-Thermal-Systems Research Unit, National Engineering School of Sfax, University of Sfax, Route de Soukra, Sfax 3038, Tunisia*
[2]*Department of Mechanical Engineering, University of Houston, Houston 77204, USA*
[3]*Applied Mechanics and Systems Research Laboratory, Tunisia Polytechnic School, University of November 7th at Carthage, B.P. 743, La Marsa 2078, Tunisia*

(Received March 4, 2007, Accepted November 17, 2009)

Abstract. This paper addresses the control issue of vibratory MEMS-based gyroscopes. This study considers a gyroscope that can be modeled by an inner mass attached to an outer mass by four springs and four dampers. The outer mass itself is attached to the rotating frame by an equal number of springs and dampers. In order to measure the angular rate of the rotating frame, a driving force is applied to the inner mass and the Coriolis force is sensed along the *y*-direction associated with the outer mass. Due to micro-fabrication imperfections, including anisoelasticity and damping effects, both gyroscopes do not allow accurate measurements, and therefore, it becomes necessary to devise feedback controllers to reduce the effects of such imperfections. Given an ideal gyroscope that meets certain performance specifications, a feedback control strategy is synthesized to reduce the error dynamics between the actual and ideal gyroscopes. For a dual-mass gyroscope, it is demonstrated that the error dynamics are remarkably decreased with the application of four actuators applied to both masses in the *x* and *y* directions. It is also shown that it is possible to reduce the error dynamics with only two actuators applied to the outer mass only. Simulation results are presented to prove the efficiency of the proposed control design.

Keywrods: control strategy; vibration; MEMS; gyroscope.

1. Introduction

The technology of micromachined accelerometers and gyroscopes has been expanded and commercialized over the past decade. Accelerometers are detection devices that produce a signal relative to a linear motion whereas gyroscopes generate a signal relative to an angular velocity or angular rotation. While accelerometers are the current leaders of the MEMS market technology, gyroscopes are expected to gain more popularity and exhibit similar success (Nasiri 2004). Micromachined gyroscopes are vibrating structures composed of an outer mass oscillating along a drive direction and an inner mass coupled with the outer one via a Coriolis force. The proof mass is suspended by elastic flexures anchored to the substrate (Acar 2004). Vibrating on the drive direction, the outer proof mass induces a Coriolis force in the sense direction so that the angular rotation becomes measurable. The oscillation in the drive mode, selected for amplifying the gyro motion and applying control forces, transforms the energy to the sense direction capable of detecting the angular rate or measuring the angular deflection (Zhuravlev 1993, Painter and Shkel 2003, Piyabongkarn *et al*. 2005).

*Corresponding Author, Professor, E-mail: sami.elborgi@gnet.tn

From all the reported gyroscopes in the literature (including Acar *et al.* 2009 and Trusov *et al.* 2009), the requirements of higher order of magnitude, improved robustness and long-term stability must be met. In fact, the micro-fabrication deficiencies and uncontrollable environmental variations affect the gyro angular deflections. As a result of structural and thermal fluctuations, these deficiencies result in the performance degradation of gyroscopes. Micromachining includes many steps to be performed: deposition process, etching process and material pattern. These processes yield performance degradation of the gyroscope since they contribute to the increase of the fabrication defects, such as anisoelasticity and anisodamping (Shkel *et al*. 1999a, Gallacher *et al*. 2005). Anisoelasticity results in frequency mismatch and mode coupling causing a disruption of the line of oscillation and exhibits an ellipsoid motion. Damping non-idealities produce zero rate output which affects the measurements by leading to precession of the line of oscillation and amplitude change (Park and Horowitz 2005). A vibrating gyroscope oscillates to reach desired amplitude, and thus, perform a transfer of energy from the drive mode to the sense mode. Then, the energy has to be kept at a constant value to measure the input angular velocity. Furthermore, the device has to cancel out the effect of quadrature error due to fabrication imperfections, and finally a measurement of the input angular velocity is performed.

To sum up, manufacturing defects such as anisoelasticity and damping affect the gyro output. For this, control techniques are necessary to cancel out the error and null the parasitic effects while maintaining a high accurate response. Generally, large imperfections which cause the interference between the measurements and the Coriolis force are trimmed by electronic components. The small perturbations are minimized by the implemented feedback control strategy. The drive combs are used to apply control forces to maintain oscillation of the proof mass while the sense combs are used to detect angular displacement and velocity.

Currently, force-balancing feedback control schemes (Yazdi *et al*. 1998, Jiang *et al*. 2000, Chang *et al*. 1998) have been widely used to cancel the effect of off-diagonal terms in the stiffness matrix which is referred to as the quadrature error, and also to increase the bandwidth and dynamic range of the gyroscope beyond the open-loop mode of operation. Park and Horowitz (2004) developed a new MEMS gyroscope operation mode and a corresponding continuous time controller determined from an adaptive control algorithm. The adaptive controlled gyroscope is self-calibrating, compensates for friction forces and fabrication imperfections that normally cause quadrature errors, and produces an unbiased angular velocity measurement that has no zero rate output. They also presented a discrete time version of the observer-based adaptive control system for MEMS gyroscopes, which can be implemented using digital process (Park and Horowitz 2005). Recently, Park *et al.* (2008) presented an algorithm for controlling vibratory MEMS gyroscopes so that they can directly measure the rotation angle without integration of the angular rate. Dong *et al*. (2008) developed a sixth order continuous-time force-feedback band-pass sigma-delta modulator control system for the detection mode of micromachined vibratory gyroscopes.

Structural anisoelasticities and nonproportional damping lead to significant modal coupling between the sense and drive modes in a resonant gyroscope, thereby reducing the accuracy of the sense output. Accurate modeling and identification of these characteristics will significantly enhance the ability to compensate for these errors via feedback/feedforward control strategies thus leading to the next generation "smart" MEMS gyroscopes with self calibrating capabilities (Painter and Shkel 2001). Piyabongkarn *et al*. (2005) have developed a composite nonlinear feedback control system that compensates for the effects of dissipative forces, mismatched springs, cross-axis stiffness and transmission of rotary torque and ensures that the gyroscope's mass behaves as a freely vibrating structure for accurate measurement of its angle and angular rate for low bandwidth applications. Shkel *et al*. (1999a) have proposed an appropriate feedback control that compensates for anisoelasticity while not interfering with the precession. Painter and

Shkel (2003) have demonstrated the necessity for a dual stage control architecture comprising feedforward and feedback control systems in order to compensate for fabrication imperfections and in-operation perturbations prevalent in micromachined gyroscopes.

In this paper, feedback control strategies are synthesized for dual-mass gyroscopes for the purpose of reducing the effects of anisoelasticity and damping coupling. The remainder of the paper is organized as follows: section 2 is concerned with the modeling and control of dual-mass gyroscopes. Simulations are presented in sections 3. Conclusions and future work are given in section 4.

2. Dynamics and control of dual mass vibratory gyroscopes

In this section, the control of a dual-mass vibratory MEMS-based gyroscope for sensing the angular rate is proposed. The gyroscope is modeled by two masses; the first mass is driven in the x-direction, and the response of the second mass is sensed along the y-axis (see Fig. 1).

It is assumed that the dynamics of the actual gyroscope is influenced by micro-fabrication imperfections resulting from system anisoelasticity and structural aero-dynamic damping. In addition, the proposed design assumes the knowledge of a reference (ideal) gyroscope that meets certain performance specifications in the time and/or frequency domains. Specifically, the sensing direction and the amplitude of vibration associated with the inner mass. In order to compensate for these imperfections, the proposed control design can be stated as follows: given the dynamics of a reference gyroscope, devise a feedback control law for the reduction of the error between the reference dynamics and that of the actual gyroscope.

2.1 Dynamics of the reference gyroscope

A dual-mass gyroscope is a lumped mass spring system. The gyro is modeled by a drive mass-active gimbal m_1 which is vibrating with small amplitudes and a slave mass-sensing plate m_2 which is oscillating at large amplitudes if the amplitude amplification design is used (Chang *et al*. 1998). The dual-mass ideal gyroscope assumes small cross-coupling damping coefficients and neglects the effect of the stiffness non-idealities. In addition, the system is undamped with isotropic suspension.

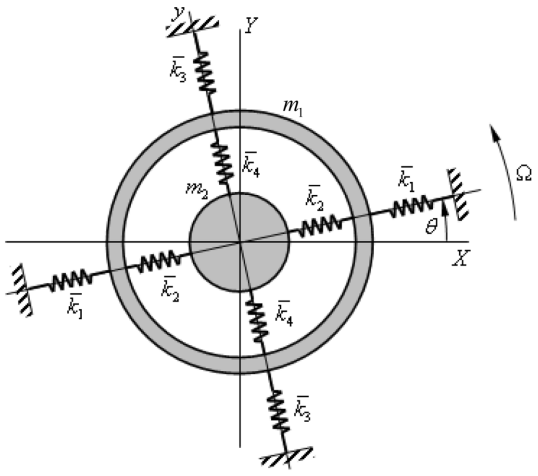

Fig. 1 A dual-mass vibratory gyroscope

The dynamics of the gyroscope is first derived using Newton's second law. Let us consider the gyro dynamics in the moving frame $\{x, y, z\}$. At any time instant t, the position vector of the center of mass of m_i ($i = 1, 2$) at time t is $\overrightarrow{OM_i}$ in the moving frame is

$$\overrightarrow{OM_i} = x_{i_r}\vec{x} + y_{i_r}\vec{y} \tag{1}$$

where $\vec{x}$ and $\vec{y}$ are unit vectors along the x and y directions, respectively. These unit vectors can be expressed in terms of the unit vectors $\vec{X}$ and $\vec{Y}$ associated with the inertial frame as

$$\vec{x} = \cos\theta\vec{X} + \sin\theta\vec{Y} \qquad \vec{y} = -\sin\theta\vec{X} + \cos\theta\vec{Y} \tag{2}$$

The absolute acceleration of mass m_i can be expressed as follows

$$\vec{a}_i = \frac{d^2\overrightarrow{OM_i}}{dt^2} + \frac{d\vec{\Omega}}{dt} \times \overrightarrow{OM_i} + \vec{\Omega} \times \vec{\Omega} \times \overrightarrow{OM_i} + 2\vec{\Omega} \times \frac{d\overrightarrow{OM_i}}{dt} \tag{3}$$

where $\vec{\Omega}$ is the input angular velocity vector. Applying Newton's second law, the equations of motion of the drive and passive masses can be written as

$$\begin{aligned} m_1\left(\frac{d^2\overrightarrow{OM_1}}{dt^2} + \frac{d\vec{\Omega}}{dt} \times \overrightarrow{OM_1} + \vec{\Omega} \times \vec{\Omega} \times \overrightarrow{OM_1} + 2\vec{\Omega} \times \frac{d\overrightarrow{OM_1}}{dt}\right) &= \overrightarrow{F_{S_1}} + \overrightarrow{F_{D_1}} \\ m_2\left(\frac{d^2\overrightarrow{OM_2}}{dt^2} + \frac{d\vec{\Omega}}{dt} \times \overrightarrow{OM_2} + \vec{\Omega} \times \vec{\Omega} \times \overrightarrow{OM_2} + 2\vec{\Omega} \times \frac{d\overrightarrow{OM_2}}{dt}\right) &= \overrightarrow{F_{S_2}} + \overrightarrow{F_{D_2}} \end{aligned} \tag{4}$$

where $\overrightarrow{F_{S_1}}$ and $\overrightarrow{F_{S_2}}$ are the spring forces and $\overrightarrow{F_{D_1}}$ and $\overrightarrow{F_{D_2}}$ the damping forces. It can be shown that the open-loop dynamics of the reference gyroscope is written as

$$\begin{aligned} &\begin{bmatrix} m_1 & 0 & 0 & 0 \\ 0 & m_1 & 0 & 0 \\ 0 & 0 & m_2 & 0 \\ 0 & 0 & 0 & m_2 \end{bmatrix} \begin{bmatrix} \ddot{x}_{1_r} \\ \ddot{y}_{1_r} \\ \ddot{x}_{2_r} \\ \ddot{y}_{2_r} \end{bmatrix} + \begin{bmatrix} \bar{c}_1 + \bar{c}_2 & -2m_1\Omega & -\bar{c}_2 & 0 \\ 2m_1\Omega & \bar{c}_3 + \bar{c}_4 & 0 & -\bar{c}_4 \\ -\bar{c}_2 & 0 & \bar{c}_2 & -2m_2\Omega \\ 0 & -\bar{c}_4 & 2m_2\Omega & \bar{c}_4 \end{bmatrix} \begin{bmatrix} \dot{x}_{1_r} \\ \dot{y}_{1_r} \\ \dot{x}_{2_r} \\ \dot{y}_{2_r} \end{bmatrix} \\ &+ \begin{bmatrix} \bar{k}_1 + \bar{k}_2 - m_1\Omega^2 & 0 & -\bar{k}_2 & 0 \\ 0 & \bar{k}_3 + \bar{k}_4 - m_1\Omega^2 & 0 & -\bar{k}_4 \\ -\bar{k}_2 & 0 & \bar{k}_2 - m_2\Omega^2 & 0 \\ 0 & -\bar{k}_4 & 0 & \bar{k}_4 - m_2\Omega^2 \end{bmatrix} \begin{bmatrix} x_{1_r} \\ y_{1_r} \\ x_{2_r} \\ y_{2_r} \end{bmatrix} = \begin{bmatrix} 1 \\ 0 \\ 0 \\ 0 \end{bmatrix} F_d \end{aligned} \tag{5}$$

or

$$M\ddot{x}_r + \bar{D}\dot{x}_r + \bar{K}x_r = \bar{B}F_d \tag{6}$$

where $\bar{c}_1$, $\bar{c}_2$, $\bar{c}_3$ and $\bar{c}_4$ are the damping coefficients (not represented in Fig. 1) $\bar{k}_1$, $\bar{k}_2$, $\bar{k}_3$ and $\bar{k}_4$ are the spring coefficients, Ω is the angular velocity, assumed to be constant in this study, $\bar{B}$ is the input vector of size 4, and F_d is the driving force applied to the outer mass. In order to guarantee sufficiently large amplitudes of the sensing mass, it is assumed that the reference gyroscope has no structural damping.

The undamped reference gyroscope ($\bar{c}_i = 0$; $i = 1,2,3,4$) is composed of 4 natural frequencies determined from

$$\det\begin{bmatrix} -\omega^2 I & -I \\ M^{-1}\bar{K} & -\omega^2 I + M^{-1}\bar{D} \end{bmatrix} = 0 \tag{7}$$

If $\bar{k}_i = \bar{k}$ ($i = 1,2,3,4$), it can be shown that the resulting undamped natural frequencies are

$$\begin{aligned} \omega_1^2, \omega_2^2 &= \frac{\bar{k}m_1 + 2\bar{k}m_2 + 2\Omega^2 m_1 m_2}{2m_1 m_2} - \frac{\bar{k}\sqrt{m_1^2 + 4m_2^2}}{2m_1 m_2} \\ &\pm\Omega\sqrt{\bar{k}\left(\frac{4}{m_1} + \frac{2}{m_2} - \frac{2m_1}{m_2\sqrt{m_1^2 + 4m_2^2}} - \frac{8m_2}{m_1\sqrt{m_1^2 + 4m_2^2}}\right)} \\ \omega_3^2, \omega_4^2 &= \frac{\bar{k}m_1 + 2\bar{k}m_2 + 2\Omega^2 m_1 m_2}{2m_1 m_2} + \frac{\bar{k}\sqrt{m_1^2 + 4m_2^2}}{2m_1 m_2} \\ &\pm\Omega\sqrt{\bar{k}\left(\frac{4}{m_1} + \frac{2}{m_2} + \frac{2m_1}{m_2\sqrt{m_1^2 + 4m_2^2}} + \frac{8m_2}{m_1\sqrt{m_1^2 + 4m_2^2}}\right)} \end{aligned} \tag{8}$$

The frequency response of the ideal gyroscope is shown in Fig. 2 ($m_1 = 5.2\times10^{-10}$ kg, $m_2 = 3.12\times10^{-10}$ kg, $\bar{k}_1 = \bar{k}_2 = \bar{k}_3 = \bar{k}_4 = 4$ Nm^{-1}, $\bar{c}_1 = \bar{c}_2 = \bar{c}_3 = \bar{c}_4 = 1.9\times10^{-6}$ N sec m^{-1}, $\Omega = 200$ rad/sec). It can be observed that at the frequency 10 KHz, the driving mass results into larger amplitude of the sensing mass. The region between the two peaks associated with the driving mass is, general, taken as the operating frequency range. More specifically, gyroscope design focuses the amplification of the time response and/or the increase of bandwidth. Depending on the objective the control strategy is different in structure.

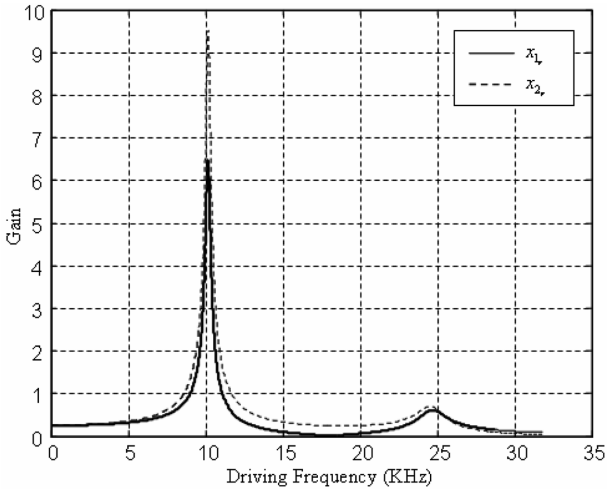

Fig. 2 Frequency response of the ideal dual-mass gyroscope

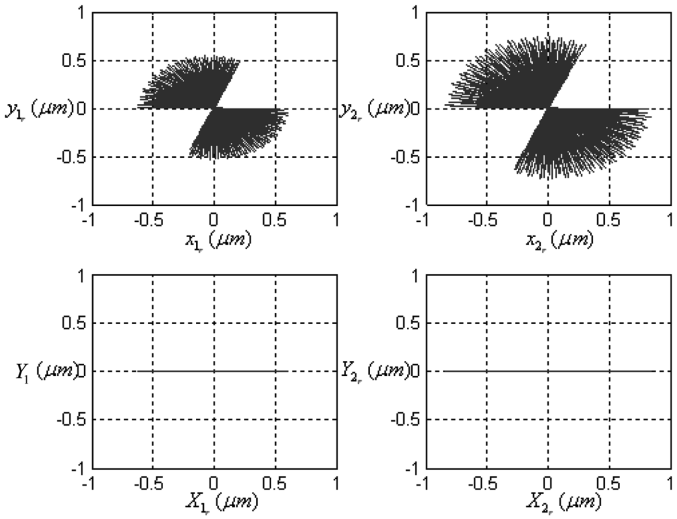

Fig. 3 Response of the ideal dual-mass gyroscope

The open-loop response of the ideal gyroscope, in both local and inertial frames, is shown in Fig. 3. The notion of angular precession holds true for both masses and a line of oscillation is associated with each. In this case, notice that the sensing plate undergoes relatively larger amplitude with respect to that of the driving gimbal mass m_1.

2.2 Dynamics of the actual gyroscope

As a result of micro-fabrication imperfections, anisoelasticity causes the line of oscillation to precess away from the physical axes of elasticity and follow the principal axis of elasticity. Anisoelasticity leads to frequency mismatch and mode coupling resulting in performance degradation (Nasiri 2004). The coefficients multiplying the position variables represent the non-ideal spring forces acting on the system rising from the lack of perfect symmetry in the gyroscope. Here, we consider a 4-DOF sense angular rates MEMS gyroscope shown in Fig. 4.

In the presence of structural aero-dynamic damping and anisoelasticity, the dynamics of the actual gyroscope is governed by the following matrix equation

$$\begin{bmatrix} m_1 & 0 & 0 & 0 \\ 0 & m_1 & 0 & 0 \\ 0 & 0 & m_2 & 0 \\ 0 & 0 & 0 & m_2 \end{bmatrix} \begin{bmatrix} \ddot{x}_{1_a} \\ \ddot{y}_{1_a} \\ \ddot{x}_{2_a} \\ \ddot{y}_{2_a} \end{bmatrix} + \begin{bmatrix} c_{x_1}+c_{x_2} & c_{xy_1}-2m_1\Omega & -c_{x_2} & 0 \\ c_{yx_1}+2m_1\Omega & c_{y_1}+c_{y_2} & 0 & -c_{y_2} \\ -c_{x_2} & 0 & c_{x_2} & c_{xy_2}-2m_2\Omega \\ 0 & -c_{y_2} & c_{yx_2}+2m_2\Omega & c_{y_2} \end{bmatrix} \begin{bmatrix} \dot{x}_{1_a} \\ \dot{y}_{1_a} \\ \dot{x}_{2_a} \\ \dot{y}_{2_a} \end{bmatrix}$$

$$+ \begin{bmatrix} k_{x_1}+k_{x_2}-m_1\Omega^2 & k_{xy_1} & -k_{x_2} & 0 \\ k_{yx_1} & k_{y_1}+k_{y_2}-m_1\Omega^2 & 0 & -k_{y_2} \\ -k_{x_2} & 0 & k_{x_2}-m_2\Omega^2 & k_{xy_2} \\ 0 & -k_{y_2} & k_{yx_2} & k_{y_2}-m_2\Omega^2 \end{bmatrix} \begin{bmatrix} x_{1_a} \\ y_{1_a} \\ x_{2_a} \\ y_{2_a} \end{bmatrix} = BF + \begin{bmatrix} 1 \\ 0 \\ 0 \\ 0 \end{bmatrix} F_d \tag{9}$$

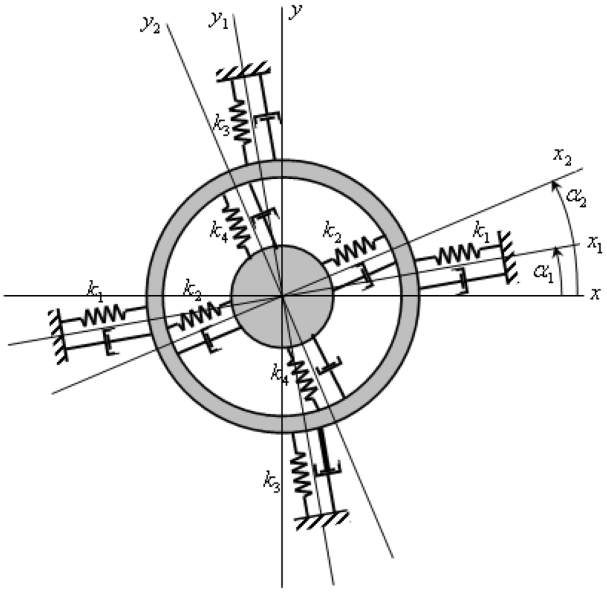

Fig. 4 Actual dual-mass gyroscope affected by anisoelasticity and damping coupling

or

$$M\ddot{x}_a + D\dot{x}_a + Kx_a = BF + \bar{B}F_d \tag{10}$$

where m_1 and m_2 are the masses, c_{x_1}, c_{y_1}, c_{x_2}, c_{y_2}, $c_{xy_1}=c_{yx_1}$ and $c_{xy_2}=c_{yx_2}$ are the damping coefficients, k_{x_1}, k_{y_1}, k_{x_2}, k_{y_2}, $k_{xy_1}=k_{yx_1}$ and $k_{xy_2}=k_{yx_2}$ are the spring coefficients, Ω is the angular velocity of the moving frame (x, y) attached to the outer mass with respect to the inertial frame (X, Y) (not shown in Fig. 4), B is the control input matrix of size $4\times m$ ($1\le m\le 4$), F is the feedback control vector of size m, and $\bar{B}$ is the input matrix associated with the driving force F_d applied to the outer mass. The device commonly operates by first driving the proof mass into forced oscillation. Upon reaching the desired amplitude, the drive force is removed and the energy of the system is maintained using the designed feedback control law F (Shkel *et al.* 1999a). The spring coefficients are given by

$$k_{x_i} = k_{n_i} + h_i \cos(2\alpha_i) \quad k_{y_i} = k_{n_i} - h_i \cos(2\alpha_i) \quad k_{yx_i} = k_{xy_i} = h_i \sin(2\alpha_i) \quad i = 1,2 \tag{11}$$

where $k_{n_1}=(k_1 + k_2)/2$ and $k_{n_2}=(k_3 + k_4)/2$ are the isotropic stiffnesses, and $h_1 = (k_1 - k_2)/2$ and $h_2 = (k_3 - k_4)/2$ are the mismatch stiffnesses along the principal axes of elasticity. Similarly, the damping coefficients are

$$c_{x_i} = c_{n_i} + d_i \cos(2\beta_i) \quad c_{x_i} = c_{n_i} - d_i \cos(2\beta_i) \quad c_{yx_i} = c_{xy_i} = d_i \sin(2\beta_i) \quad i = 1,2 \tag{12}$$

where $c_{n_1} = (c_1 + c_2)/2$, $c_{n_2} = (c_3 + c_4)/2$ are the ideal damping coefficients, $d_1 = (c_1 - c_2)/2$ and $d_2 = (c_3 - c_4)/2$ are the cross-damping terms, and β_i (not shown in Fig. 4) is the angle between the physical axes and principal axes of damping.

The uncontrolled response of the dual-mass gyroscope is shown in Fig. 5 ($\Omega = 200$ rad/s, $m_1 = 5.2\times10^{-10}$ kg, $m_2 = 3.12\times10^{-10}$ kg, $k_1 = 4$ N/m, $k_2 = 3.8$ N/m, $k_3 = 3.9$ N/m, $k_4 = 3.8$ N/m, $c_1 = 1.2\times10^{-8}$ N sec/m,

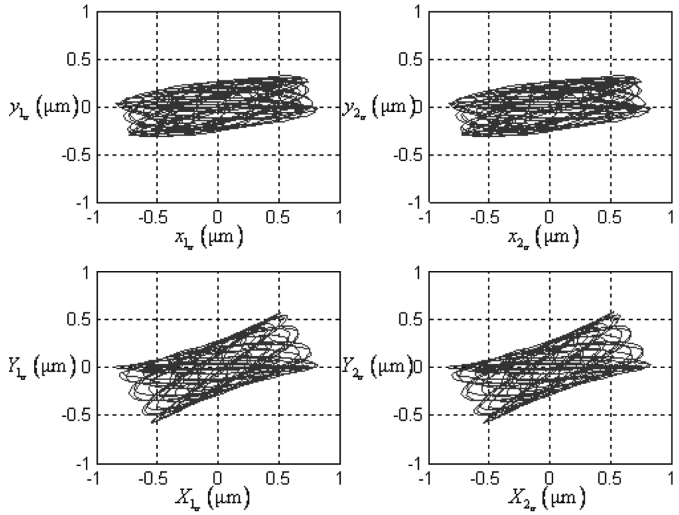

Fig. 5 Motion of the inner and outer masses in the moving and inertial frames

$c_2 = 0.25\times10^{-8}$ N sec/m, $c_3 = 1.933\times10^{-8}$ N sec/m, $c_4 = 0.68\times10^{-8}$ N sec/m, $\alpha_1 = \pi/36$, $\alpha_2 = \pi/54$, $\beta_1 = \pi/72$, and $\beta_2 = \pi/36$). Plots show an erratic pattern of oscillation manifested in an elliptic pattern bounded by a parallelogram.

As shown in the figures above, the line of oscillation is disturbed due to the effect of non-idealities and the motion is more amplified in the drive mass compared to the sensing plate. Thus, the imperfections shift the natural frequencies and lead to variations in the motion of each mass. To quantify the performance difference between the ideal and actual gyroscopes, let $\varepsilon_{x_i} = x_{a_i} - x_{r_i}$ and $\varepsilon_{y_i} = y_{a_i} - y_{r_i}$ ($i = 1,2$) be the errors in the x_i and y_i-directions, respectively. For control purposes, an augmented system can be constructed using Eqs. (6) and (10). We get

$$\begin{bmatrix} M & 0 \\ 0 & M \end{bmatrix}\begin{bmatrix} \ddot{x}_a \\ \ddot{\varepsilon} \end{bmatrix} + \begin{bmatrix} \bar{D} + \delta D & 0 \\ \delta D & \bar{D} \end{bmatrix}\begin{bmatrix} \dot{x}_a \\ \dot{\varepsilon} \end{bmatrix} + \begin{bmatrix} \bar{K} + \delta K & 0 \\ \delta K & \bar{K} \end{bmatrix}\begin{bmatrix} x_a \\ \varepsilon \end{bmatrix} = \begin{bmatrix} B \\ B \end{bmatrix} F + \begin{bmatrix} \bar{B} \\ 0 \end{bmatrix} F_d \tag{13}$$

where

$$x_a = \begin{bmatrix} x_{1_a} \\ y_{1_a} \\ x_{2_a} \\ y_{2_a} \end{bmatrix} \quad x_r = \begin{bmatrix} x_{1_r} \\ y_{1_r} \\ x_{2_r} \\ y_{2_r} \end{bmatrix} \quad \varepsilon = \begin{bmatrix} \varepsilon_{x_1} \\ \varepsilon_{y_1} \\ \varepsilon_{x_2} \\ \varepsilon_{y_2} \end{bmatrix}$$

The damping and stiffness matrices D and K associated with the actual gyroscope are assumed to be expressed by $\bar{D} + \delta D$ and $\bar{K} + \delta K$, respectively. The matrices δD and δK characterize the deviations from the ideal device due to imperfections. Simulations of the open-loop dynamics show that the steady-state error cannot be brought faster to zero due to the effect of anisoelasticity (see Fig. 6). A feedback control force is thus required to compensate for these errors. For this, we propose two types of feedback control strategy. The first is based on the Lyapunov technique and the second is constructed using optimal control.

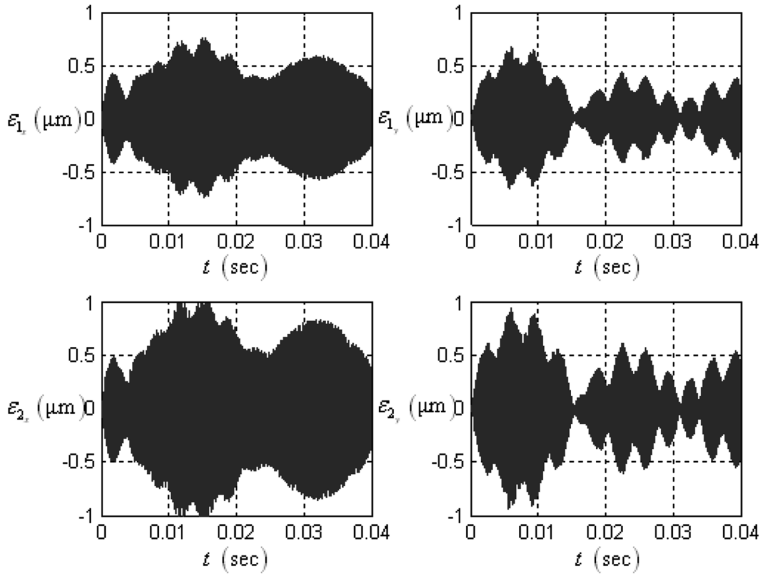

Fig. 6 The error is not regular

2.3 Lyapunov-based control

In this section, we propose a Lyapunov-based control design for the reduction of the dual-mass gyroscope sensitivity to micro-fabrication imperfections. Eq. (11) reveals that the error dynamics can be written as

$$M\ddot{\varepsilon} + \overline{D}\dot{\varepsilon} + \overline{K}\varepsilon = -\delta D\dot{x}_a - \delta K x_a + BF \tag{14}$$

or

$$M\ddot{\varepsilon} + (\overline{D} + \delta D)\dot{\varepsilon} + (\overline{K} + \delta K)\varepsilon = -\delta D\dot{x}_i - \delta K x_i + BF \tag{15}$$

Therefore, for small anisoelasticity and damping effects, the error stability is linked to system (M, $\overline{D}$, $\overline{K}$). For this, we propose to use the following Lyapunov energy function

$$L = \frac{1}{2}\dot{\varepsilon}^T M\dot{\varepsilon} + \frac{1}{2}\varepsilon^T\overline{K}\varepsilon \tag{16}$$

The time derivative of the Eq. (16) suggests that the controller (B is set to the identity matrix) be in the following form

$$\begin{Bmatrix} F_{x1} \\ F_{y1} \\ F_{x2} \\ F_{y2} \end{Bmatrix} = -\begin{bmatrix} 2\xi_1 m_1\omega_1 & 0 & 0 & 0 \\ 0 & 2\xi_2 m_1\omega_2 & 0 & 0 \\ 0 & 0 & 2\xi_3 m_2\omega_3 & 0 \\ 0 & 0 & 0 & 2\xi_4 m_2\omega_4 \end{bmatrix}\begin{bmatrix} \dot{\varepsilon}_{x1} \\ \dot{\varepsilon}_{y1} \\ \dot{\varepsilon}_{x2} \\ \dot{\varepsilon}_{y2} \end{bmatrix} \tag{17}$$

where ω_i (i = 1,2,3,4) are the ideal gyro's natural frequencies and ξ_1, ξ_2, ξ_3 and ξ_4 are damping ratios. The resulting performance is shown in Figs. 7 and 8. It is clear that the errors are remarkably reduced

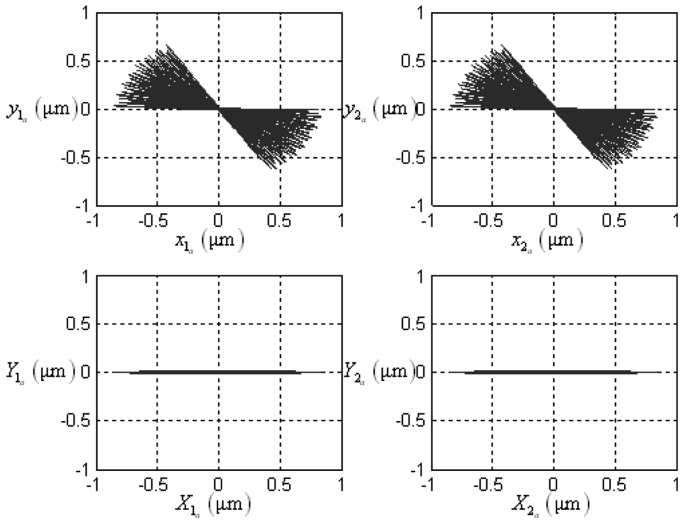

Fig. 7 Controlled motion of the actual gyroscope

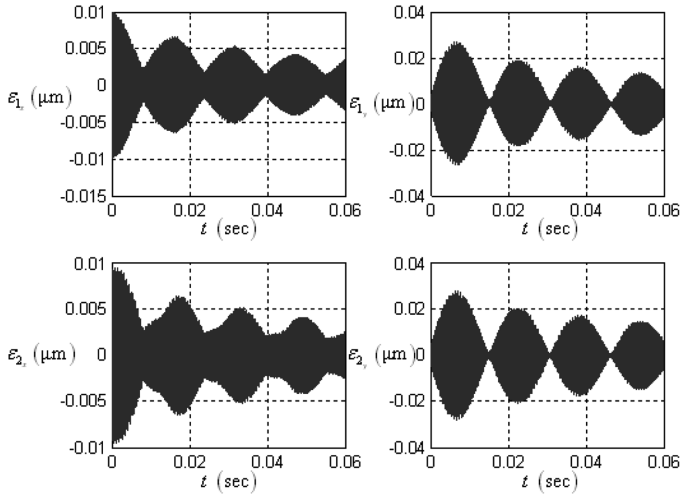

Fig. 8 Controlled errors of the actual gyroscope

with the proposed control strategy, and thus, the actual gyroscope tracks the ideal dynamics. The remaining constant amplitude of the error is due to the effect of the feedforward term presented in Eq. (15) leading to the appearance of the beating phenomena.

It can be noticed that the aforementioned control structure uses a full feedback control (use of 4 actuators). The advantage of the above control is that its structure is simple since the control law is made of 4 independent derivative control forces. In the next section, we develop a different control strategy in which the number of actuators is addressed.

2.4 Optimal control

This section is concerned with the design of an optimal control strategy with the aim of stabilizing the

closed-loop dynamics of the dual-mass gyroscope and reducing the error amplitude during precession. In the presence of structural damping and anisoelesticity, the error dynamics is governed by the following equation

$$M\ddot{\varepsilon}+(\overline{D}+\delta D)\dot{\varepsilon}+(\overline{K}+\delta K)\varepsilon = -\delta D\dot{x}_i-\delta Kx_i+HF \tag{18}$$

or

$$\begin{bmatrix} m_1 & 0 & 0 & 0 \\ 0 & m_1 & 0 & 0 \\ 0 & 0 & m_2 & 0 \\ 0 & 0 & 0 & m_2 \end{bmatrix}\begin{bmatrix} \ddot{\varepsilon}_{x1} \\ \ddot{\varepsilon}_{y1} \\ \ddot{\varepsilon}_{x2} \\ \ddot{\varepsilon}_{y2} \end{bmatrix}+\begin{bmatrix} c_{x1}+c_{x2} & c_{xy1}-2m_1\Omega & -c_{x2} & 0 \\ c_{xy1}+2m_1\Omega & c_{y1}+c_{y2} & 0 & -c_{y2} \\ -c_{x2} & 0 & c_{x2} & c_{xy2}-2m_2\Omega \\ 0 & -c_{y2} & c_{xy2}+2m_2\Omega & c_{y2} \end{bmatrix}\begin{bmatrix} \dot{\varepsilon}_{x1} \\ \dot{\varepsilon}_{y1} \\ \dot{\varepsilon}_{x2} \\ \dot{\varepsilon}_{y2} \end{bmatrix}$$
$$+\begin{bmatrix} k_{x1}+k_{x2} & k_{xy1} & -k_{x2} & 0 \\ k_{xy1} & k_{y1}+k_{y2} & 0 & -k_{y2} \\ -k_{x2} & 0 & k_{x2} & k_{xy2} \\ 0 & -k_{y2} & k_{xy2} & k_{y2} \end{bmatrix}\begin{bmatrix} \varepsilon_{x1} \\ \varepsilon_{y1} \\ \varepsilon_{x2} \\ \varepsilon_{y2} \end{bmatrix}=-\delta D\dot{x}_i-\delta Kx_i+HF \tag{19}$$

We notice that the error stability is clearly affected by the damping and anisoelasticity coupling terms δD and δK. Therefore, to reduce the effect of these imperfections, a control technique should be synthesized. However, if the error dynamics is stabilized via the feedback gains, it may not be possible to drive it to the zero steady state because of the effects of damping and anisoelasticity. Consequently, the task of the optimal control design is to guarantee both stability and tracking in the presence of micro-fabrication imperfections where δD and δK are considered as parameter uncertainties affecting gyroscope damping and stiffness.

Since MEMS-based gyroscopes operate at high frequency (in the order of some KHz), one may be faced with numerical problems using modern softwares, such as Matlab and Mathematica, to calculate the feedback gains. It is then necessary to introduce a scaling factor α for the time variable. It is given by

$$t=\alpha\tau \tag{20}$$

Substitution of Eq. (20) in (18) leads to

$$\frac{1}{\alpha^2}M\varepsilon''+\frac{1}{\alpha}\left(\overline{D}+\delta D\right)\varepsilon'+\left(\overline{K}+\delta K\right)\varepsilon=-\frac{1}{\alpha}\delta Dx_i'-\delta Kx_i+HF \tag{21}$$

where the prime denotes $d\cdot/d\tau$ and

$$\ddot{\varepsilon} = \frac{1}{\alpha^2}\varepsilon'' \tag{22}$$

The optimal control gains are determined from the following dynamics (characterizing the ideal dynamics)

$$\bar{\varepsilon}' = A\bar{\varepsilon}+BF \tag{23}$$

where

$$A=\begin{bmatrix} 0_{4x4} & I_{4x4} \\ -\alpha^2M^{-1}\overline{K} & -\alpha M^{-1}\overline{D} \end{bmatrix} \quad B=\alpha^2M^{-1}\begin{bmatrix} 0_{4x2} \\ H \end{bmatrix} \quad \bar{\varepsilon}=\begin{bmatrix} \varepsilon \\ \dot{\varepsilon} \end{bmatrix}$$

The control force vector $F = K\bar{\varepsilon}$ minimizes the performance index

$$J = \frac{1}{2}\int_0^\infty (\bar{\varepsilon}^T Q\bar{\varepsilon} + F^T RF)dt$$

the solution of which is obtained by solving the following algebraic Riccati equation

$$A^T Z + ZA - 0.5ZBR^{-1}B^T Z + 2Q = 0 \tag{24}$$

Thus, the gain matrix K is determined from

$$K = -0.5R^{-1}B^T Z \tag{25}$$

Therefore, the resulting feedback control force can be put in the following form

$$F = K\bar{\varepsilon} = [K_1 \;\; K_2]\begin{bmatrix}\varepsilon \\ \varepsilon'\end{bmatrix} = K_1\varepsilon + K_2\varepsilon' \tag{26}$$

Using the time variable t, the feedback control law (26) can be rewritten as

$$F = K_1\varepsilon + \alpha K_2\dot{\varepsilon} \tag{27}$$

At this stage, a practical issue of importance is the number of actuators employed in the control design. Of course, reducing the number of actuators is preferred at the implementation phase. We shall consider three design cases. In the first case, a set of four forces are applied to both masses (two actuators assigned to each in the x and y directions). The second case assumes two forces applied to the outer gimbal in both x and y directions. Finally, a third case considers the application of a single force to the outer gimbal in the x direction only. All cases aim at reducing the sensitivity of the dual gyroscope to micro-fabrication imperfections. In others words the three design cases are defined as follows

(i) four actuators $H = I_{4\times 4}$ $\quad F = \begin{bmatrix}F_{x1} \\ F_{y1} \\ F_{x2} \\ F_{y2}\end{bmatrix}$

(ii) two actuators $H = \begin{bmatrix}1 & 0 \\ 0 & 1 \\ 0 & 0 \\ 0 & 0\end{bmatrix}$ $\quad F = \begin{bmatrix}F_{x1} \\ F_{y1}\end{bmatrix}$

(iii) one actuator $H = \begin{bmatrix}1 \\ 0 \\ 0 \\ 0\end{bmatrix}$ $\quad F = F_{x1}$

2.4.1 Optimal control with four actuators

In this part, we shall consider the use of four actuators for driving the actual gyroscope to track the ideal

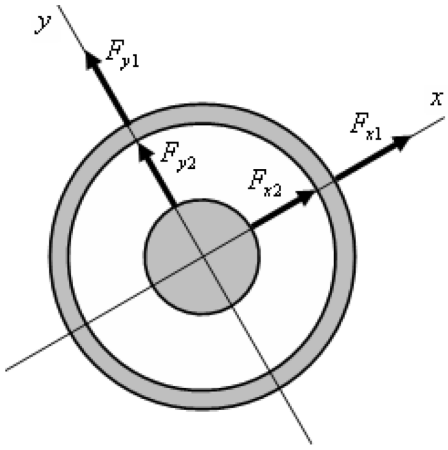

Fig. 9 Distribution of 4 actuators

dynamics. The actuator distribution is as shown in Fig. 9.

In this case, at each mass, two control forces are applied along the drive and sense directions. Therefore, the optimal control strategy yields the system performance displayed in Figs. 10 and 11. It can be seen that the controlled error of the dual mass rate integrating gyroscope is reduced, and thus, the actual gyroscope tracks the ideal dynamics.

Though the employment of the optimal control method using four actuators yields satisfactory results, the implemented algorithm seems to be costly. Therefore, investigation of an optimal control using two actuators is sought in the following section.

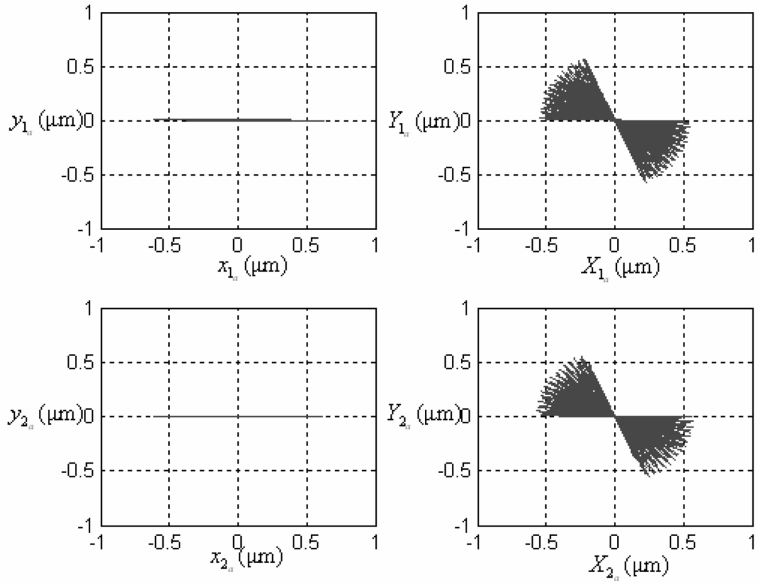

Fig. 10 Controlled motion of both the outer and the inner mass the actual gyroscope

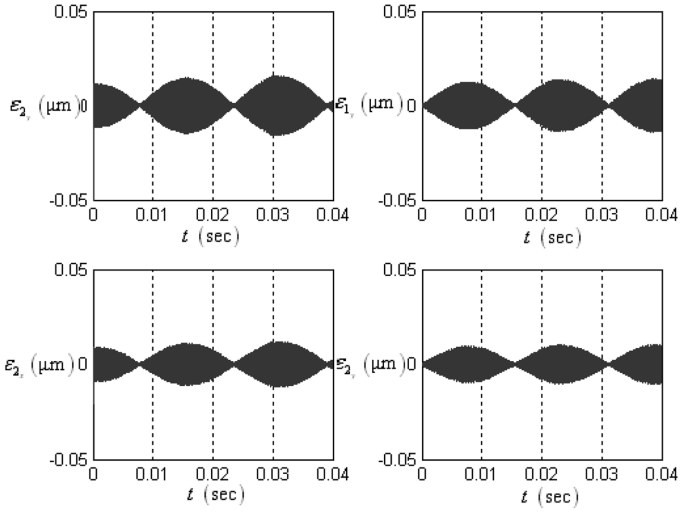

Fig. 11 Controlled error of the actual gyroscope

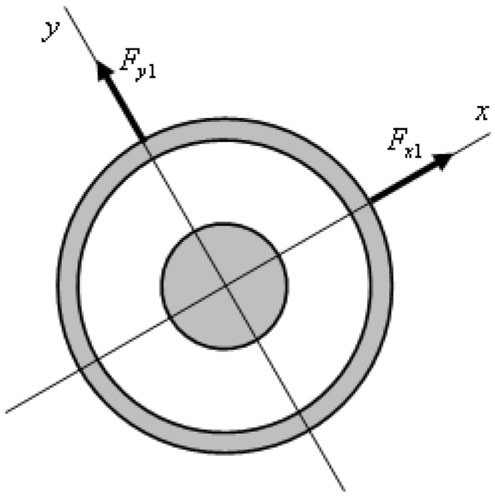

Fig. 12 Distribution of 2 actuators

2.4.2 Optimal control with two actuators

In this section case, two actuators are applied to the driving gimbal as shown in Fig. 12.

The applied optimal control leads to the time response shown in Figs. 13 and 14. As compared to the first case, two actuators led to a slightly larger error. However, the global response of the gyroscope tracks well the ideal dynamics. It can be seen that two actuators suffice to control the dual-mass system, and therefore, represents a solution to the problem of reducing the number of actuators in the gyroscope design.

2.4.3 Optimal control with a single actuator

Finally, this study seeks the possibility of using a single actuator applied to the driving gimbal along the x direction as depicted in Fig. 15.

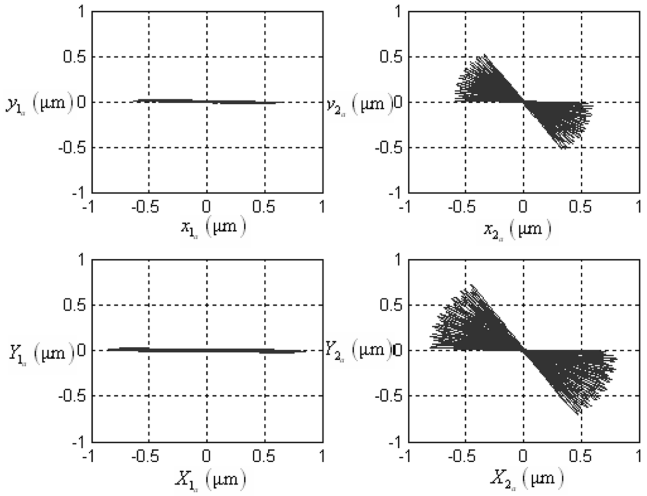

Fig. 13 Controlled motion of the outer mass and inner mass of the actual gyroscope

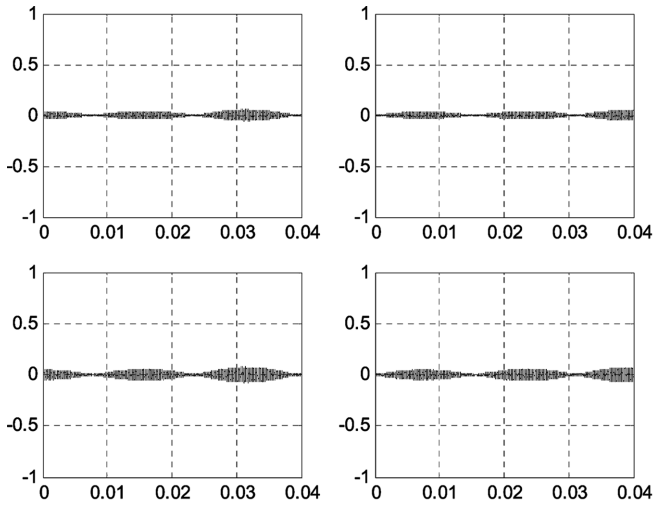

Fig. 14 Controlled error of the actual gyroscope

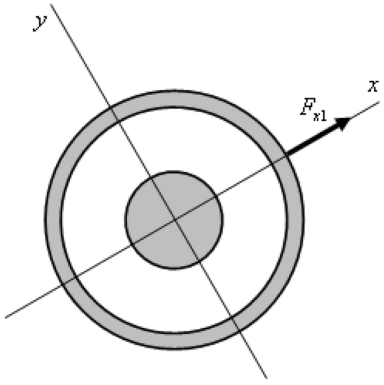

Fig. 15 The use of a single actuator

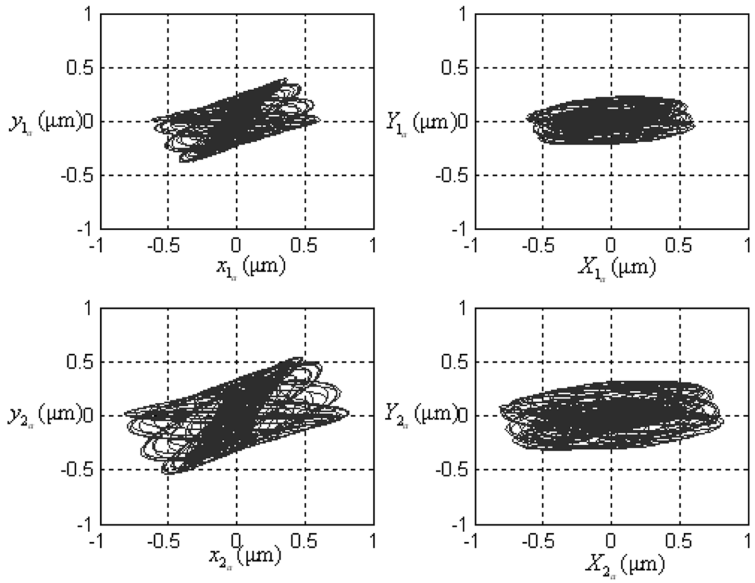

Fig. 16 Response of the actual gyroscope to a single actuator

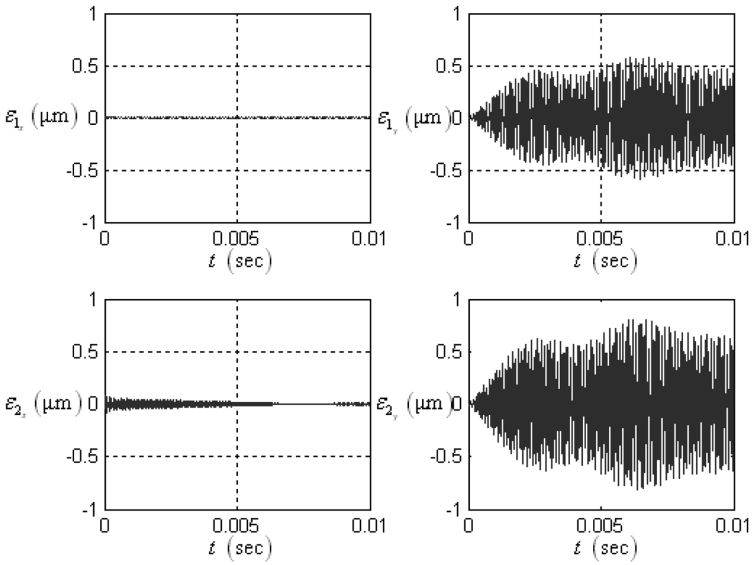

Fig. 17 Error response of the actual gyroscope to a single actuator

The resulting performance of the dual-mass gyroscope is shown in Figs. 16 and 17. Though, the error in the drive direction is drastically reduced, a single actuator fails to reduce effectively the error in the y direction.

3. Conclusions

This paper presented the control design of vibratory dual-mass MEMS-based gyroscopes. Due to micro-fabrication imperfections, including anisoelasticity and damping effects, these gyroscopes do not allow accurate measurements of the angular velocity and displacement. For this, feedback controllers were devised to reduce the effects of such imperfections. The design consisted of two steps. First, an ideal gyroscope was designed to meet certain performance specifications. Second, two feedback control strategies were synthesized to reduce the error dynamics between the actual and ideal gyroscopes. Using both strategies, it was shown that the error dynamics of dual-mass gyroscopes was remarkably decreased with the application of four actuators applied to both masses in the drive and sense directions. It was also demonstrated that, using the second control strategy, it was possible to reduce the error dynamics with only two actuators applied to the outer mass only. Simulation results were presented to prove the efficiency of the proposed control designs.

Acknowledgements

The authors would like to thank the comments and suggestions made by Professor Andrei M. Shkel, of the University of California at Irvine for improving the quality of this paper. The first and third authors are grateful for the funding provided to their laboratories by the Tunisian Ministry of Higher Education and Scientific Research.

References

Acar, C. (2004), *Robust vibratory gyroscopes*, PhD thesis, Department of aerospace and mechanical engineering, University of California at Irvine, USA.

Acar, C., Schofield, A.R., Trusov, A.A., Costlow, L.E. and Shkel, A.M. (2009), "Environmentally robust MEMS vibratory gyroscopes for automotive applications", *IEEE Sens. J.*, **9**(12), 1895-1906.

Chang, S., Chia, M., Castillo-Borelley, P., Higdon, W., Jiang, Q., Johnson, J., Obedier, L., Putty, M., Shi, Q., Sparks, D. and Zarabadi, S. (1998), "An electroformed CMOS integrated angular rate sensor", *Sensor. Actuat. A-Phys.*, **66**(1-3), 138-143.

Dong, Y., Kraft, M., Hedenstierna, N. and Redman-White, W. (2008), "Microgyroscope control system using a high-order band-pass continuous-time sigma-delta modulator", *Sensor. Actuat. A-Phys.*, **145-146**, 299-305.

Gallacher, B.J., Hedley, J., Burdess, J.S., Harris, A.J., Rickard, A. and King, D.O. (2005), "Electrostatic correction of structural imperfections present in a microring gyroscope", *J. Microelectromech. S.*, **14**(2), 221-234.

Jiang, X., Seeger, J.I., Kraft, M. and Boser, B.E. (2000), "A monolithic surface micromachined z-axis gyroscope with digital output", *Proceedings of the IEEE 2000 Symposium on VLSI Circuits, Digest of Technical Papers*, Honolulu, HI, USA.

Nasiri, S. (2004), *A critical review of MEMS gyroscopes technology and commercialization status*, Invensense.

Painter, C.C. and Shkel, A.M. (2003), "Active structural error suppression in MEMS vibratory rate integrating gyroscopes", *IEEE Sens. J.*, **3**(5), 595-606.

Painter, C.C. and Shkel, A.M. (2001), "Identification of anisoelasticity for electrostatic trimming of rate integrating gyroscope", *Proceedings of the SPIE Annual International Symposium on Smart Structures and Materials*, New Port Beach, CA., USA, March.

Park, S. and Horowitz, R. (2004), "New adaptive mode of operation for MEMS gyroscopes", *J. Dyn. Syst. Meas. Control*, **126**(4), 800-810.

Park, S. and Horowitz, R. (2005), "Discrete time adaptive control for a MEMS gyroscope", *Int. J. Adapt. Control*

Signal Process., **19**(6), 485-503.
Park, S., Horowitz, R. and Tan, C.W. (2008), "Dynamics and control of a MEMS angle measuring gyroscope", *Sensor. Actuat. A-Phys.*, **144**, 56-63.
Piyabongkarn, D., Rajamani, R. and Greminger, M. (2005), "The development of a MEMS gyroscope for absolute angle measurement", *IEEE T. Contr. Syst. T.*, **13**(2), 185-195.
Shkel, A.M., Horowitz, R., Seshia, A.A., Park, S. and Howe, R.T. (1999a), "Dynamics and control of micromachined gyroscopes", *Proceedings of the American Control Conference*, San Diego, CA, USA, June.
Shkel, A.M., Howe, R.T., Horowitz, R. (1999b), "Modeling and simulation of micromachined gyroscopes in the presence of imperfection", *Proceedings of the International Conference on Modelling and Simulation of Microsystems,* Puerto Rico, USA.
Trusov, A.A., Schofield, A.R. and Shkel, A.M. (2009), "Performance characterization of a new temperaturerobust gain-bandwidth improved MEMS gyroscope operated in air", *Sensor. Actuat. A-Phys*., **155**(1), 16-22.
Yazdi, N., Ayazi, F. and Najafi, K. (1998), "Micromachined inertial sensors", *P. IEEE*, **86**(8), 1640-1659.
Zhuravlev, V.F. (1993), "Theoretical foundation of solid state wave gyroscope", *Mech. Solids*, **28**(3), 3-15.

CC